Deep radio observations of 3C 324 and 3C 368: evidence for jet–cloud interactions

P. N. Best,[1] C. L. Carilli,[2] S. T. Garrington,[3] M. S. Longair[4] and H. J. A. Röttgering[1]

[1]*Sterrewacht Leiden, Huygens Laboratory, PO Box 9513, 2300 RA Leiden, The Netherlands*
[2]*NRAO, PO Box 0, Socorro, NM 87801-0387, USA*
[3]*The University of Manchester, NRAL, Jodrell Bank, Lower Withington, Macclesfield, Cheshire, SK11 9DL*
[4]*Cavendish Labs, Madingley Road, Cambridge, CB3 0HE*

ABSTRACT

High-resolution, deep radio images are presented for two distant radio galaxies, 3C 324 ($z = 1.206$) and 3C 368 ($z = 1.132$), which are both prime examples of the radio–optical alignment effect seen in powerful radio galaxies with redshifts $z \gtrsim 0.6$. Radio observations were made using the Very Large Array in A-array configuration at 5 and 8 GHz, and using the MERLIN array at 1.4 and 1.65 GHz. Radio spectral index, radio polarization, and rotation measure maps are presented for both sources.

Radio core candidates are detected in each source, and by aligning these with the centroid of the infrared emission the radio and the optical / infrared images can be related astrometrically with 0.1 arcsec accuracy. In each source the radio core is located at a minimum of the optical emission, probably associated with a central dust lane. Both sources also exhibit radio jets which lie along the directions of the bright strings of optical knots seen in high-resolution *Hubble Space Telescope* images. The northern arm of 3C 368 shows a close correlation between the radio and optical emission, whilst along the jet direction of 3C 324 the bright radio and optical knots are co-linear but not co-spatial. These indicate that interactions between the radio jet and its environment play a key role in producing the excess ultraviolet emission of these sources, but that the detailed mechanisms vary from source to source.

3C 368 is strongly depolarized and has an average rest-frame rotation measure of a few hundred rad m^{-2}, reaching about 1000 rad m^{-2} close to the most depolarized regions. 3C 324 has weaker depolarization, and an average rest-frame rotation measure of between 100 and 200 rad m^{-2}. Both sources show large gradients in their rotation measure structures, with variations of up to 1000 rad m^{-2} over distances of about 10 kpc.

Key words: polarization – galaxies: active – galaxies: jets – infrared: galaxies – radio continuum: galaxies.

1 INTRODUCTION

The discovery that the optical, ultraviolet and line emission of powerful high-redshift radio galaxies is elongated and aligned along the direction of the radio axis (McCarthy et al. 1987; Chambers et al. 1987), a phenomenon known as the 'alignment effect', indicates a close association between radio source activity and the optical emission of these galaxies. A number of processes have been proposed to account for these radio–optical correlations (see McCarthy 1993 for a review), the most promising models falling into two broad categories: interaction models in which the correlations arise directly through interactions between the radio jet and its environment, and illumination models in which radiation from a partially obscured active galactic nucleus (AGN) both photoionizes the emission-line gas within an ionization cone and

is scattered by dust grains or electrons producing the optical and ultraviolet alignment.

One of the earliest models for the alignment effect, which has remained popular, is star formation induced by the passage of the radio jets (e.g. Rees 1989). This process has been observed in jet–cloud interactions at low redshifts, for example in Minkowski's object (Brodie, Bowyer & McCarthy 1985; van Breugel et al. 1985) and in the radio lobe of 3C 285 (van Breugel & Dey 1993). There is quite convincing evidence that it also occurs in at least some distant radio galaxies (e.g. Best et al. 1997a; Dey et al. 1997) but, as yet, direct evidence for the presence of young stars in the aligned structures is limited.

A large proportion of the powerful distant radio galaxies which have been studied using spectropolarimetry have optical emission which is polarized at up to the 15 per cent level, and scattered broad

lines in their spectra (e.g. Dey & Spinrad 1996; Cimatti et al. 1996, 1997, and references therein). A significant proportion of the aligned emission of these galaxies must therefore be scattered light from an obscured AGN. In an optically unbiased sample of distant radio galaxies, however, Tadhunter et al. (1997) detected significant polarization in only 40 per cent of the galaxies although most showed large ultraviolet excesses.

Nebular continuum emission provides another important alignment mechanism. Dickson et al. (1995) showed that a combination of free–free, free–bound, and two-photon continuum, as well as the Balmer forest, can contribute a significant proportion (5–40 per cent) of the ultraviolet emission from the nuclear regions of powerful radio galaxies, and this may be even higher in the extended aligned emission regions (e.g. Stockton, Ridgway & Kellogg 1996). Since either or both of photoionization by the AGN and shock-ionization by the radio jet may be responsible for exciting the gas, distinguishing between the jet–cloud interaction model and the illumination model is made more difficult.

The structure and properties of the radio emission from these distant radio galaxies can offer important clues to the nature of the radio–optical correlations. *Hubble Space Telescope* (*HST*) observations of 28 radio galaxies at redshifts $z \sim 1$, selected from the revised 3CR catalogue of Laing, Riley & Longair (1983), have shown that for the majority of small radio sources the alignment effect manifests itself in the form of strings of bright knots tightly aligned between the two radio lobes (Best, Longair & Röttgering 1996, 1997b). Deep, high-resolution radio observations of these sources provide a critical test of the interaction/illumination models: if the locations of the radio jets and the strings of optical activity are co–linear, then the influence of the radio jets must play a key role in the alignment effect. This would not, however, provide direct proof of the jet-induced star formation hypothesis: the emission may be nebular continuum emission from warm gas shocked by the radio jets, or may be associated with an increased scattering efficiency in these regions, for example by jet shocks breaking up cold gas clouds and exposing previously hidden dust grains, thereby increasing the surface area for scattering along the jet axis (Bremer, Fabian & Crawford 1997).

One of the major problems in interpreting the radio–optical structures of distant radio galaxies has been accurate relative astrometry of the radio and optical/infrared frames of reference. Radio observations are automatically in the International Celestial Reference Frame (ICRF), with positional errors of about 0.01 arcsec, but the absolute positions of the *HST* images are uncertain at the 1 arcsec level (Lattanzi, Capetti & Macchetto 1997). Such astrometric uncertainties mean that bright radio knots may be either correlated or anti-correlated with the position of the luminous optical emission regions. This problem can be alleviated somewhat by multifrequency radio observations of sufficient sensitivity to detect a flat-spectrum central radio core: this core is expected to be coincident with the nucleus of the galaxy, which itself is located roughly at the centroid of the infrared image of the galaxy. The optical (rest-frame ultraviolet) emission cannot be used for this procedure, since it is often severely affected by both dust extinction (e.g. de Koff et al. 1996; Best et al. 1997b) and the aligned emission. The infrared images also contain a component of aligned emission (e.g. Eisenhardt & Chokshi 1990; Rigler et al. 1992; Dunlop & Peacock 1993; Best et al. 1997b,1998) but at a significantly lower level, and are seen to show a sharp central peak, which can be astrometrically aligned with the radio core.

It should be noted that this process can never be 100 per cent reliable, owing to the ambiguity of identifying radio core

components based upon spectral index information alone; the case of 3C 356 (Fernini et al. 1993; Best et al. 1997a) is a case in point. For the radio galaxies in the current paper, however, further radio–optical correlations are observed when this process is employed (see Sections 3 and 4), indicating that the core identifications are most likely correct.

The properties of the radio emission also provide a probe of the large-scale physical environment of the radio source. There has been growing evidence that powerful radio galaxies at large redshifts lie in rich (proto-) cluster environments, based upon measures of galaxy cross-correlation functions (e.g. Yates, Miller & Peacock 1989), detections of powerful extended X-ray emission from the vicinity of distant radio sources (e.g. Crawford & Fabian 1996), detections of companion galaxies in narrow-band images and with spectroscopy (e.g. Dickinson et al. 1997; McCarthy 1988), and the very bright infrared magnitudes and large characteristic sizes of the radio galaxies themselves, suggesting that they are as large and luminous as brightest cluster galaxies (see Best, Longair & Röttgering 1998 for a review). Radio data provide further evidence in support of this hypothesis. At low redshifts, radio galaxies in rich cluster environments, such as Cygnus A, tend to have very large rotation measures, $RM \gtrsim 1000 \, \text{rad m}^{-2}$ (Dreher, Carilli & Perely 1987; Taylor, Barton & Ge 1994). Carilli et al. (1997) have studied a sample of 37 radio galaxies with redshifts $z > 2$, and detect rotation measures exceeding $1000 \, \text{rad m}^{-2}$ in 19 per cent of them. They consider this percentage to be a conservative lower limit, and interpret these large rotation measures as arising from hot, magnetized (proto-)cluster atmospheres surrounding the sources, with field strengths $\sim 1 \, \text{nT}$. Detailed studies of individual sources with very high rotation measures support this interpretation (Carilli, Owen & Harris 1994; Pentericci et al. 1997). In comparison with these very distant sources, the polarization properties of radio galaxies with redshift $z \sim 1$ have not been well studied at high angular resolution (although see Pedelty et al. 1989, Liu & Pooley 1991, Fernini et al. 1993, and Johnson, Leahy & Garrington 1995).

We have selected two radio galaxies from the 3CR sample, with redshifts in excess of one: 3C 324 ($z = 1.206$) and 3C 368 ($z = 1.132$). These galaxies are both prime examples of the alignment effect; their *Hubble Space Telescope* (*HST*) images show highly extended optical morphologies with strings of bright knots close to the radio axis (Longair, Best & Röttgering 1995). We have carried out sensitive, multifrequency, polarimetric radio observations of these radio sources at high angular resolution using the VLA and MERLIN. A description of the observations and the data reduction techniques is given in Section 2. In Section 3, we present the radio data for 3C 324, and make a comparison with the optical and infrared images. This is repeated for 3C 368 in Section 4. These sources are compared in Section 5, in which we also summarize our conclusions. Throughout the paper we assume $H_0 = 50 \, \text{km s}^{-1} \, \text{Mpc}^{-1}$ and $\Omega = 1$, and all positions are given in equinox J2000 coordinates.

2   OBSERVATIONS AND DATA REDUCTION

2.1   Very Large Array (VLA) observations

Observations of 3C 324 and 3C 368 were made in 1995 July, in the 5- and 8-GHz bands of the VLA in A–array configuration. 3C 368 was also observed in the 1.4-GHz band. Details of the observations are given in Table 1.

The observations were made using standard VLA procedures. Primary flux calibration was achieved using the bright source

Table 1. The parameters of the radio observations.

Source	Redshift	Observation Date	Interferometer	Frequencies [MHz]	Bandwidth [MHz]	Integration Time [min]	Map rms noise [μJy/beam]	Restoring beam FWHM [arcsec]
3C 324	1.206	11th July 1995	VLA	4535, 4885	50	77	26	0.40
			VLA	8085, 8335	50	291	13	0.22
3C 368	1.132	31st July 1995	VLA	1465, 1515	50	120	51	1.35
			VLA	4535, 4885	50	60	25	0.45
			VLA	8085, 8335	50	123	20	0.23
		3rd March 1996	MERLIN	1658	15×1	780	119	0.23×0.15
		16th March 1996	MERLIN	1420	15×1	780	150	0.25×0.16

3C 286, and the nearby secondary calibrators 1513+236 and 1824+107 were observed regularly to provide accurate phase calibration for 3C 324 and 3C 368 respectively. The observations of these calibrators, spaced over a wide range of parallactic angles, also determined the on-axis antenna polarization response terms. Scans of 3C 286, separated in time by 6 h, provided absolute polarization position angle calibration. The uncertainty in the calibration of the position angles, estimated from the difference between the solutions for the scans of 3C 286, was about ± 2 deg at each frequency. For observations at 4710 and 8210 MHz, this corresponds to an uncertainty in the absolute value of the rotation measure of about 20 rad m^{-2}.

The data were reduced using the AIPS software provided by the National Radio Astronomy Observatory. The two IFs of the 8-GHz band data were combined to provide a single data set at 8210 MHz and those in the 1.4 GHz band were combined at 1490 MHz. The different IFs of the 5-GHz band data were reduced separately. The data were CLEANed, and phase self-calibration was used to improve the map quality. The calibration was generally very successful, yielding images with off-source noise levels within 50 per cent of the expected theoretical values.

2.2 MERLIN observations

3C 368 was observed by MERLIN at 1420 and 1658 MHz, with the parameters of the observations provided in Table 1. The run at 1420 MHz was made without the Wardle telescope, and the Mk2 telescope was used as the home-station telescope at Jodrell Bank. The total track length of each run was 13 h, and the data were recorded in 15×1 MHz bandwidth channels.

Initial amplitude and bandpass calibration were carried out using 2134+004 and 0552+398, whose flux densities were determined by comparison with 3C 286. Further phase and amplitude calibration was carried out using 1752+119, which was observed for 2 min every 10 min throughout the run and was assumed to be unresolved. This source was also used to determine the instrumental polarization to within 0.5 per cent. A short observation of 3C 286 provided absolute polarization position angle calibration.

Images of 3C 368 were then made separately at each of the two frequencies, and several cycles of self-calibration in AIPS and also in DIFMAP (Shepherd 1997) were used to improve the final image quality.

2.3 Images

For both sources, images were made at full angular resolution in the Stokes parameters I, Q and U at each frequency, by CLEANing the

final data sets using the AIPS task IMAGR with the data weighting parameter ROBUST set to zero. The FWHM of the Gaussian restoring beams are listed in Table 1. The Stokes I images of the two IFs in the 5-GHz band were combined to produce a single 4710 MHz total intensity image.

To produce maps of spectral index, rotation measure, and depolarization, observations at different frequencies must be matched in their uv-coverage and beam size. Images of the 8-GHz data were therefore created at the lower resolution of the 5-GHz data, by applying an upper cut-off in the uv data matching the longest baseline sampled at 5 GHz, together with uv tapering to retain the smooth coverage of the uv plane. The CLEANed components were restored using a Gaussian beam appropriate for the 5-GHz data. The resulting images were then checked against the 5-GHz images for any astrometric differences between the positions of the hotspots, resulting from the self-calibration procedure. No offsets in excess of 0.1 arcsec were found.

Spectral index maps (where we define the spectral index, α, as $I_\nu \propto \nu^{-\alpha}$) were made for both sources using these 8210-MHz matched-resolution total intensity maps and the combined 4710-MHz total intensity maps. Spectral index values were only calculated for regions of the images with surface brightness in excess of 5σ at both frequencies, where σ is the rms noise level of the image. Rotation measures were derived using the position angle of the polarized intensity at the three frequencies 4535, 4885 and 8210 MHz. Rotation measures were only derived in regions of the source for which polarized intensity was detected in excess of 4σ at all three frequencies. The fractional polarization at each frequency was derived by dividing the flux density determined from the total polarized intensity map, after correction for noise bias, by the flux density of the total intensity map, and is therefore a scalar rather than vector average of the polarization. The depolarization measure, $DM_{8.2}^{4.7}$, defined as the ratio of the fractional polarization at 4710 MHz to that at 8210 MHz, was derived only in regions of the source where the polarized intensity in both images exceeded 4σ.

3 3C 324

3.1 Radio properties of the source

Fig. 1(a) shows the 8210-MHz total intensity contour map of 3C 324, and Fig. 1(b) shows the corresponding 4710-MHz total intensity map with vectors of the radio polarization overlaid. A grey-scale map of the spectral index calculated between these two frequencies, as described in Section 2.3, is shown in Fig. 1(c) with contours of the 4710-MHz radio emission overlaid. The source can be separated into four components: the western lobe, the eastern lobe, a central knot, and a knot close to the western lobe. The
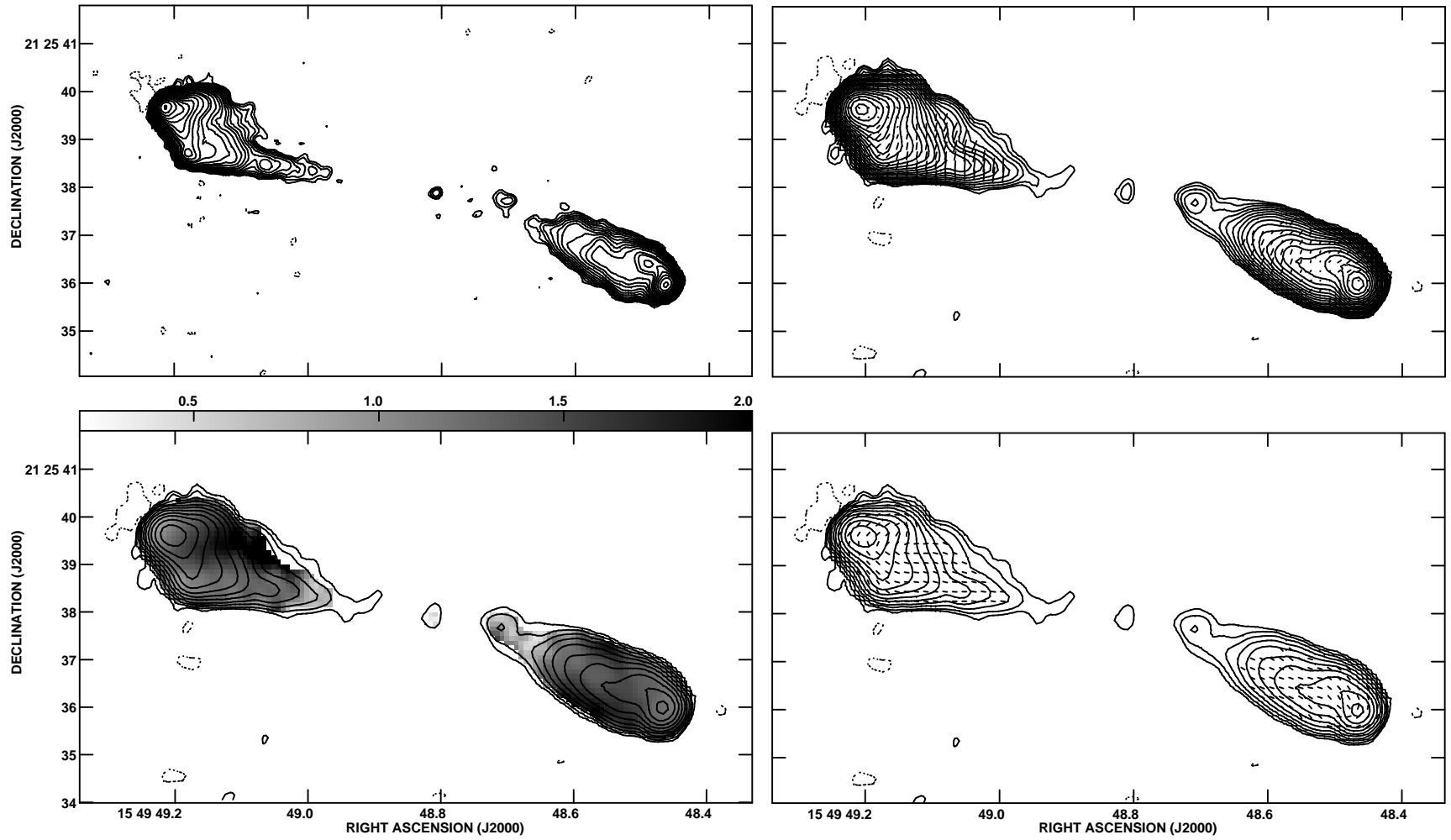
Figure 1. Maps of the radio source 3C 324 (a - upper left) 8210-MHz total intensity map. Contours are logarithmic, with a ratio of $\sqrt{2}$, beginning at 45 μJy beam^{-1}. (b - upper right) 4710-MHz total intensity map, with vectors of fractional polarization overlaid. Contours of the radio map are logarithmic, with a ratio of $\sqrt{2}$, beginning at 85 μJy beam^{-1}. A vector of length 0.4 arcsec corresponds to 100 per cent polarization. (c - lower left) The spectral index map, calculated between 4710 and 9210 MHz. (d - lower right) The magnetic field position angle, plotted wherever a rotation measure could be calculated.
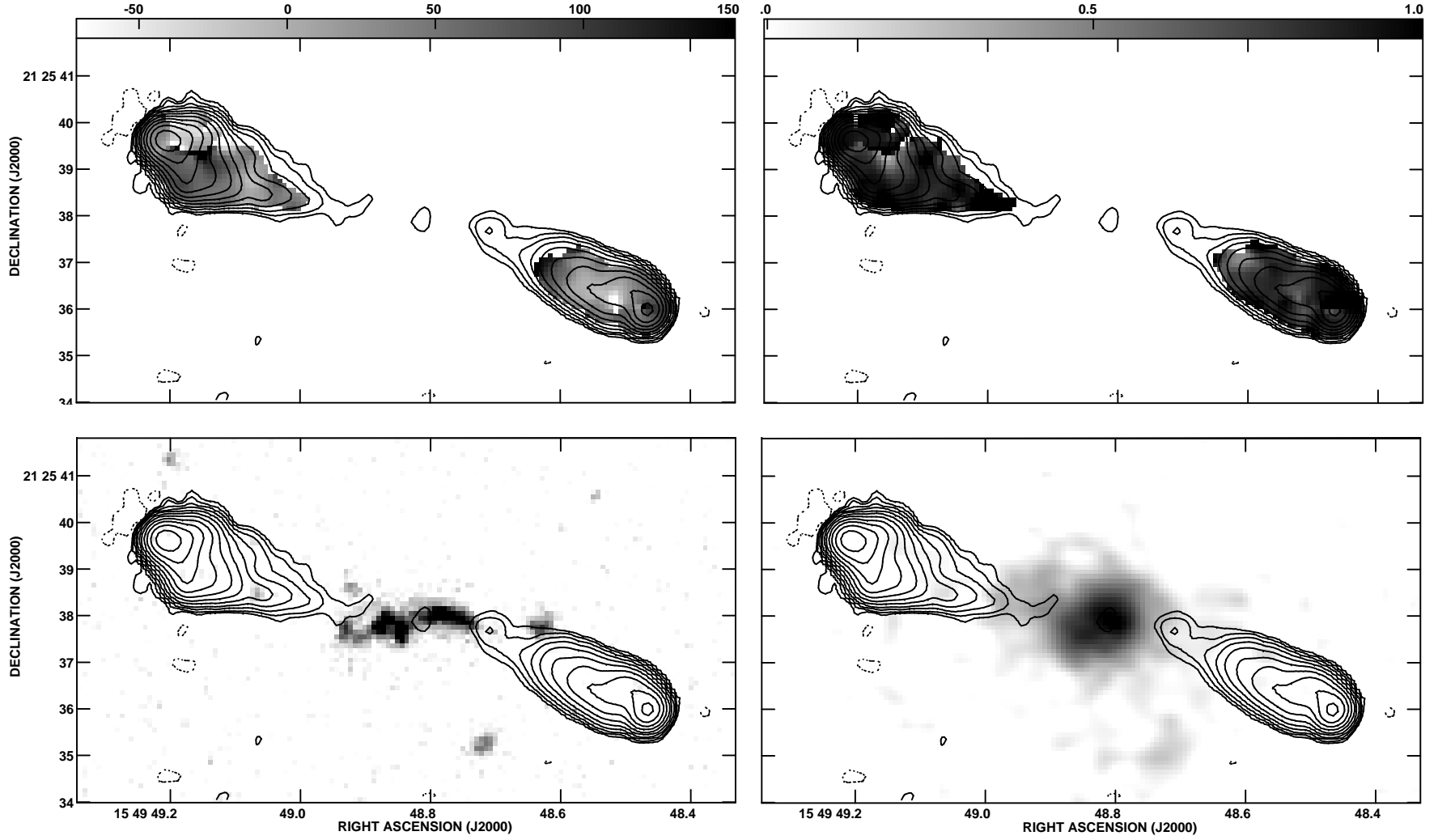
Figure 1 – *continued*. (e - upper left) A rotation measure map of the source, calculated from the frequencies 4535, 4885 and 8210 MHz. (f - upper right) A map of the depolarization measure between 8210 and 4710 MHz. (g - lower left) The sum of two WFPC2 *HST* images of 3C 324, each of duration 30 min, taken through filters F702W and F791W (see Best et al. 1997b). (h - lower right) A 54-min K-band image of 3C 324, taken with the IRCAM3 array of UKIRT (see Best et al. 1997b). The contours of radio emission at 4710 MHz overlaid on figures (c) through to (h) are logarithmic with a ratio of 2 beginning at 95 μJy beam $^{-1}$.

Table 2. Global properties of the various components of the two sources. The spectral index and depolarization measures listed are those calculated between 4710 and 8210 MHz. The rotation measures are the mean values for a region of the source as calculated from the three frequencies 4535, 4885 and 8210 MHz. The 'global' depolarization measures are calculated by first determining the scalar fractional polarization at the two frequencies and then dividing.

Source	Region	Total intensity 8210 MHz [mJy]	Fractional Polarization 8210 MHz [per cent]	Total intensity 4710 MHz [mJy]	Fractional Polarization 4710 MHz [per cent]	Total intensity 1490 MHz [mJy]	Fractional Polarization 1490 MHz [per cent]	Spec. index α	Depolar. measure $DM_{8.2}^{4.7}$	Rotation measure RM [rad m^{-2}]
3C 324	Whole	332	18.1	686	15.8	—	—	1.31	0.88	41
	W lobe	93	17.2	196	15.1	—	—	1.34	0.87	45
	E lobe	238	17.8	489	15.6	—	—	1.30	0.88	38
	Core	0.14	—	0.17	—	—	—	0.30	—	—
	W knot	0.74	—	1.00	—	—	—	0.54	—	—
3C 368	Whole	98	9.6	229	6.7	1205	1.1	1.52	0.70	85
	N lobe	47	9.9	109	8.2	564	0.6	1.51	0.83	100
	S lobe	50	9.8	118	5.4	641	1.5	1.55	0.55	63
	Core	0.16	—	0.22	—	—	—	0.54	—	—
	S knot	0.28	—	0.55	—	—	—	1.22	—	—

integrated radio properties of these four regions are listed separately in Table 2. The central knot has a spectral index of 0.30, significantly flatter than the rest of the source. Although the cores of low-redshift radio sources tend to have very flat spectra, those seen in radio sources with redshifts $z \gtrsim 1.5$ often have somewhat steeper spectra (Lonsdale, Barthel & Miley 1993; Carilli et al. 1997; Athreya et al. 1997), and so a spectral index of 0.3 for a radio core at redshift $z \sim 1$ is not unreasonable. We therefore identify this knot with the active galactic nucleus.

In the high angular resolution observations at 8 GHz, a radio jet is detected passing through a series of knots along the southern edge of the eastern lobe and then making a dramatic 55° turn to the north at the eastern end of the lobe. In Fig. 1(d), we show a map of the magnetic field position angle; these vectors lie parallel to the jet direction along this string of knots, and echo the sharp turn northwards (see also the polarization position angle in Fig. 1b). The relatively flat spectral index of this region of the radio source (Fig. 1c) adds further support to this picture. The north-western region of this eastern lobe has a steep spectral index, characteristic of ageing lobe electrons (Scheuer & Williams 1968).

To the west of the core no clear radio jet is detected, although the knot of radio emission along this axis has a relatively flat spectral index, $\alpha \approx 0.54$, and may be a jet knot. This knot lies directly upon a line from the jet in the eastern lobe through the radio core. Interestingly, the hotspots of the western and eastern lobes and the radio core are approximately co-linear, although this line is misaligned by 10° from the current axis of the radio jet.

In Fig. 1(e), a map of the rotation measure is shown, calculated as described in Section 2.3. The mean rotation measures of the eastern and western lobes are 38 and 45 rad m^{-2} respectively, only about twice the 1σ limit for a secure detection (see Section 2.1). There is, however, considerable structure in the rotation measure map, the rotation measure changing from about −50 to about +150 rad m^{-2} over an angular scale of order one arcsec; such gradients are unlikely to be of Galactic origin (Leahy 1987). Thus, the observed values for the rotation measures must be scaled up by a factor of $(1+z)^2$, or 4.87, and so the variations in the rest-frame rotation measure for 3C 324 approach 1000 rad m^{-2} over distances of about 10 kpc.

The regions of the highest rotation measure are associated with regions in which the strongest depolarization is observed between 8210 and 4710 MHz in Fig. 1(f). The observed values for the

depolarization and rotation measures can be compared if it is assumed that the depolarization results from a Gaussian distribution of Faraday depths within each beamwidth. If the standard deviation of that Gaussian distribution is Δ, measured in rad m^{-2}, then the polarization, m_λ at a given wavelength is given by the depolarization law of Burn (1966):

$$m_\lambda = m_0 \exp[-2\Delta^2\lambda^4]. \tag{1}$$

For observations at 4710 and 8210 MHz, this gives

$$\Delta = 185(1+z)^2 \left[-\ln DM_{8.2}^{4.7}\right]^{0.5} \tag{2}$$

which for 3C 324 yields $\Delta \sim 320$ rad m^{-2}, comparable to the range of rotation measures observed. These correlations between the depolarization and the gradient of the rotation measures suggest that the Faraday screen is external, arising from gas surrounding the radio lobes.

3.2 Radio–optical correlations

In Fig. 1(g), we show an *HST* image of 3C 324, with the radio contours from the 4710 MHz observation overlaid. The *HST* image represents the sum of two 30-min observations, taken through the F702W and F791W filters of WFPC2 (Longair et al. 1995). In Fig. 1(h), we show a 54-min *K*-band image of the source taken using IRCAM3 of UKIRT in 1 arcsec seeing. The *HST* and UKIRT images were astrometrically aligned using a number of unresolved objects appearing on both frames. These were then aligned with the radio data assuming that the radio core is coincident with the centre of the infrared image, providing an astrometric accuracy of approximately 0.1 arcsec. The details of these *HST* and UKIRT images have been extensively discussed elsewhere (Best et al. 1997b); here we consider only their relation to the new radio data.

The most striking feature of Fig. 1(g) is that the regions of bright radio and optical emission are co-linear, but not co-spatial. The radio core is located at a minima in the optical emission, probably associated with a central dust lane of extinction $E(B-V) \gtrsim 0.3$ (Longair et al. 1995; Dickinson, Dey & Spinrad 1996). To the west of this, a string of bright optical knots curve round towards the western radio knot; at the end of this curve they point directly towards the western radio hotspot. There is no bright optical emission coincident with the radio knot, but beyond this there lies a further optical knot. In the eastern arm of the radio source, the

optical knots do not form such a smooth structure, but the radio jet becomes luminous where the bright optical emission ceases. The apparent rotation of the axis of 3C 324 with decreasing size, from that defined by the radio hotspots, through that defined by the radio jet, to that defined by the optical emission has been interpreted by Dickinson et al. (1996) as being associated with precession of the axis of the AGN. The sharp bend of the radio jet in the eastern arm would then represent a location where the jet makes a glancing impact upon the cocoon wall (Cox, Gull & Scheuer 1991).

The UKIRT image (see also the *K*-band map of Dunlop & Peacock 1993) has significantly lower angular resolution but, intriguingly, it shows faint emission in the eastern radio lobe close to the region which shows a large gradient in the rotation measure and where the depolarization is strongest. These features may be associated with a companion galaxy to 3C 324. A deeper, high-resolution image is required to confirm this.

4 3C 368

4.1 Radio properties of the source

Fig. 2(a) shows the VLA 8210-MHz total intensity contour map of 3C 368, and Fig. 2(b) the corresponding 4710-MHz intensity map. A MERLIN 1658-MHz map is given in Fig. 2(c). Fig. 2(d) shows a grey-scale map of the spectral index between 4710 and 8210 MHz, overlaid with a contour map of the 8-GHz radio emission made at the lower resolution of the 5-GHz data (see Section 2.3).

Fig. 2(a) shows two unresolved central components. The integrated properties of each of these knots and of the northern and southern radio lobes are listed in Table 2. The southern of these two knots has been previously detected by Djorgovski et al. (1987) and Chamber, Miley & Joyce (1988), and associated by these authors with the radio core. However, our observations indicate that the spectral index of this knot is $\alpha \approx 1.22$, much steeper than would be expected of a radio core. The northern knot, detected here for the first time, has a much flatter spectral index, $\alpha \approx 0.54$, more consistent with the core spectral indices that might be expected at this redshift (see the discussion in Section 3.1). Furthermore, the 5-GHz and lower resolution 8-GHz radio maps (Figs 2b and d) show a clear jet structure leading from this northern knot to the northern radio lobe, supporting this hypothesis. In the following discussion, we assume the northern knot is associated with the AGN.

Overlaid upon Fig. 2(b), we show the polarization vectors of the source at 5 GHz. Perhaps the most striking features are the very low levels of polarization detected in each of the radio lobes with, in particular, no polarized emission being detected from the northern half of the southern lobe. Where significant polarization is detected, the magnetic field vectors are oriented parallel to the radio jet directions (see Fig. 2i). Fig. 2(e) shows the depolarization measure calculated between 8210 and 4710 MHz; the depolarization of the northern lobe is strong, but relatively constant, whilst the southern lobe shows a steep gradient of strengthening depolarization towards the north. This is demonstrated in Fig. 3(a) where the depolarization measures between 8210 and 4710 MHz, and between 4710 and 1420 MHz at the same angular resolution, are plotted as a function of declination throughout the southern lobe. It is apparent that the depolarization strengthens to the north.

In the regions where polarized emission is detected, the rotation measure has been calculated from the 4535, 4885 and 8210 MHz observations as described in Section 2.3, and is shown in Fig. 2(f). The global rotation measures of the northern and southern lobes are

100 and 63 rad m^{-2} respectively. The northern radio lobe shows little structure in the rotation measure map, but the southern lobe shows large gradients in its rotation measure, mirroring the variations in depolarization measure: the rotation measure is relatively constant throughout the southern half of the lobe (variations $\lesssim 20$ rad m^{-2}), and then increases dramatically towards the north-east and decreases dramatically towards the north-west. Because the high and low rotation measures in the north-east and north-west corners arise from regions where the polarization is low, to confirm that the values are real, in Fig. 4 we plot the polarization position angle against wavelength squared from 8 to 1.4 GHz, averaged throughout these two regions and through the 'constant RM' area in the south of the lobe. The position angles, allowing for $n\pi$ ambiguities, are well fit by a λ-squared law across all five wavelengths in each of these three locations, with rotation measures of 88 rad m^{-2} for the southern region of the lobe (dotted line), 224 rad m^{-2} for the north-eastern corner (dashed line), and -36 rad m^{-2} for the north-western corner (solid line). This confirms the large variations in the rotation measure.

3C 368 lies at moderately low galactic latitude ($b = 15°$), and so we cannot exclude a galactic origin for rotation measures of about 100 rad m^{-2}. However, the large gradients in the rotation measure and the correlation between the depolarization and rotation measure structures indicate that they are more likely to be associated with Faraday rotation by matter local to 3C 368. The measured rotation measures must therefore be scaled up by a factor of $(1 + z)^2$, or 4.55, giving mean rest-frame rotation measures for the northern and southern lobes of 455 and 263 rad m^{-2} respectively, with the southern lobe rotation measure changing from about -160 to about 1000 rad m^{-2} over a distance of less than 10 kpc. Furthermore, the large gradient in depolarization measure towards the northern end of the southern lobe suggests that the lack of polarized emission at 8 GHz from this region of the source is likely to be due this region of the source having been strongly depolarized, and thus the intrinsic rotation measure values for that region might be very large.

Using equation (2), we can estimate the expected dispersion in rotation measure values if the depolarization is associated with variations in the Faraday depth of material within each beamwidth; this gives $\Delta \sim 680$ rad m^{-2} for the southern lobe and $\Delta \sim 360$ rad m^{-2} for the northern lobe, again comparable to the observed values. The depolarization expected between 4.7 and 1.4 GHz by Burn's law (equation 1) for these values of Δ is far larger than observed. This is consistent with the slower fall-off of depolarization with wavelength predicted by Tribble (1991) for an external Faraday screen with rotation measure variations on a scale comparable to the beam size, and supports the hypothesis that the depolarization and Faraday rotation occur in a external Faraday screen local to the radio source.

4.2 Radio−optical correlations

In Figs 2(g) and (h), the radio emission of 3C 368 is compared with the optical and infrared emission. Fig. 2(g) shows total intensity 5-GHz radio contours overlaid upon the grey-scale *HST* image of the source presented by Longair et al. (1995). This image is a combination of two 30-min *HST* exposures taken through the F702W and F791W filters. Fig. 2(h) shows the same radio contours overlaid upon an infrared '*H* + *K*' image kindly provided by Alan Stockton; this is a 7200-s exposure through a combined *H* and *K*-band filter taken with the University of Hawaii 2.2-m telescope, with an angular resolution of 0.32 arcsec.
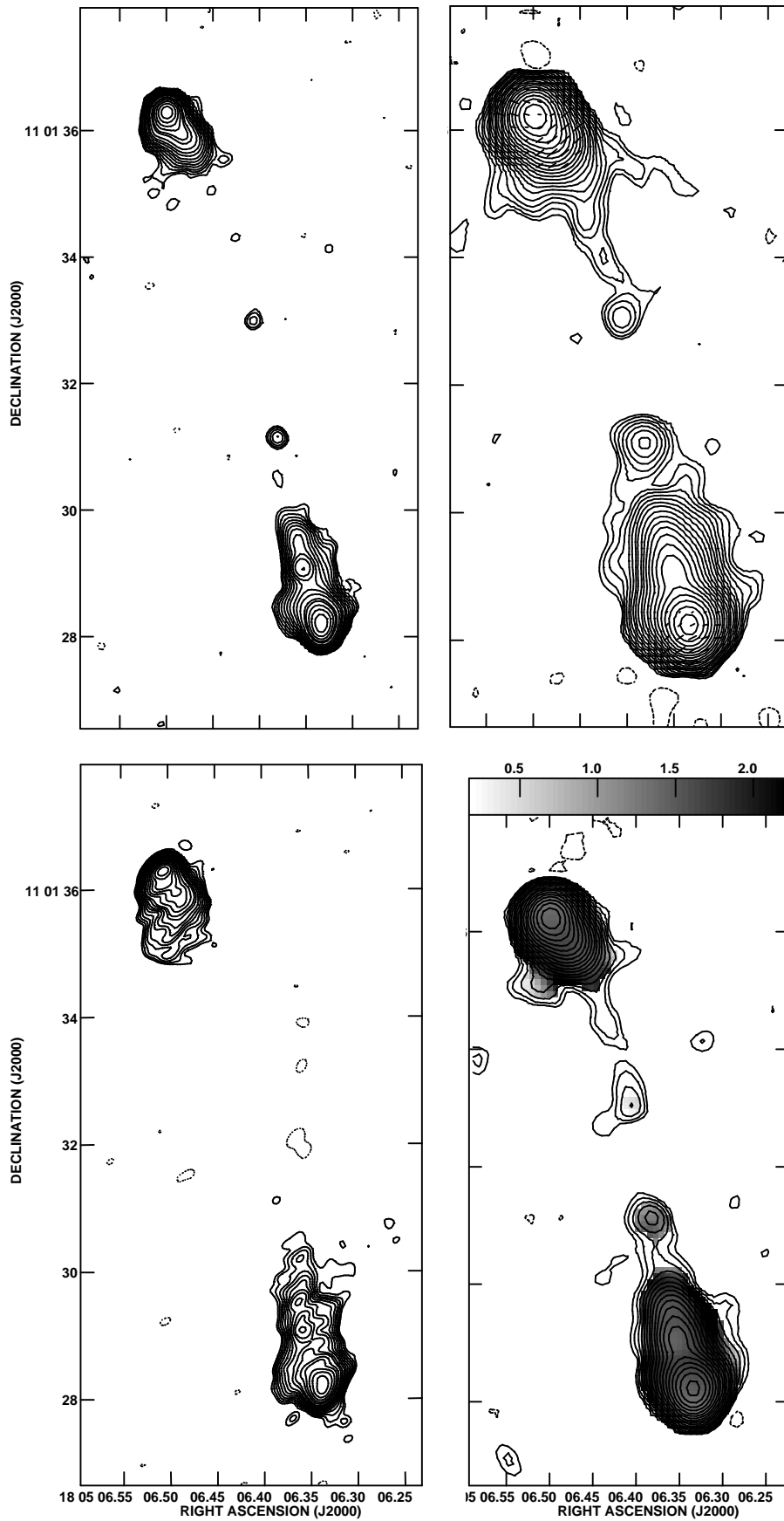
Figure 2. Panels (a) upper left, (b) upper right, (c) lower left and (d) lower right.
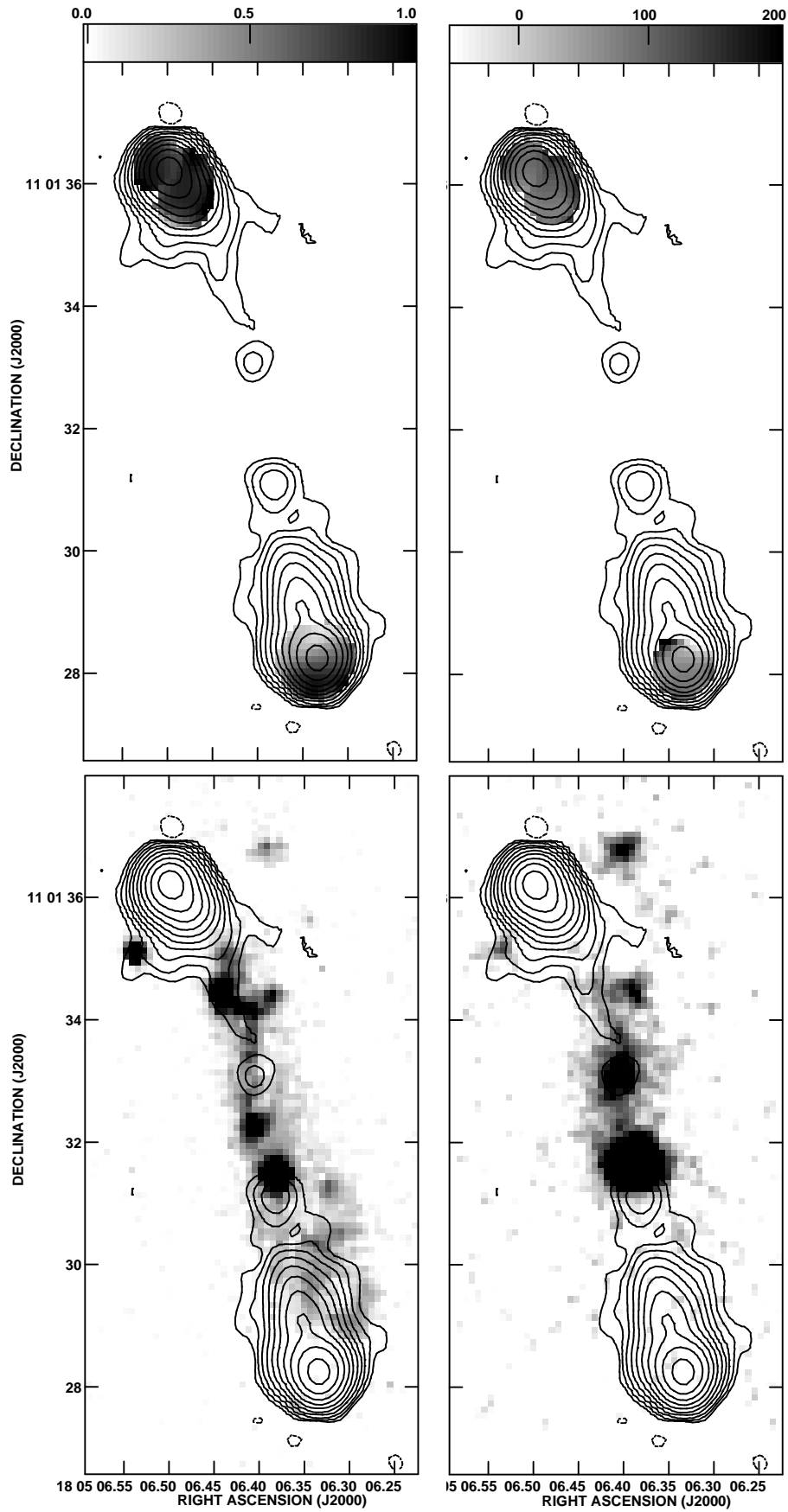
Figure 2. Panels (e) upper left, (f) upper right, (g) lower left and (h) lower right.
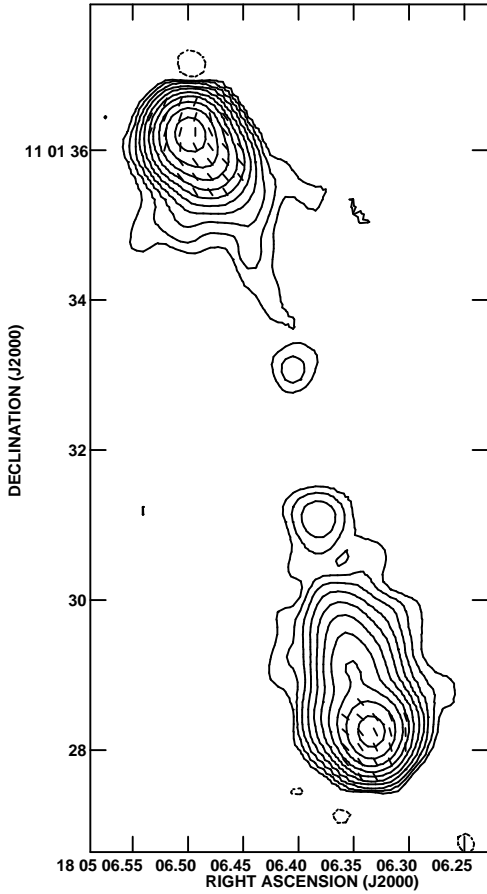
Figure 2. Maps of the radio source 3C 368 (a) 8210-MHz total intensity map. Contours are logarithmic with a ratio of $\sqrt{2}$, beginning at 60 μJy beam^{-1}. (b) 4170-MHz total intensity map, with vectors of fractional polarization overlaid. The radio contours are logarithmic, with a ratio of $\sqrt{2}$, beginning at 65 μJy beam^{-1}. A vector of length 1.0 arcsec corresponds to 100 per cent polarization. (c) The 1658-MHz MERLIN map, with logarithmic radio contours with a ratio of $\sqrt{2}$, beginning at 500 μJy beam^{-1}. (d) The spectral index map, calculated between 4710 and 8210 MHz, overlaid with contours of the 8-GHz radio emission at the resolution of the 5-GHz data. Contour levels are logarithmic, with a ratio of $\sqrt{2}$, beginning at 60 μJy beam^{-1}. (e) A map of the depolarization measure between 8210 and 4710 MHz. (f) A rotation measure map of the source, calculated from the frequencies 4535, 4885 and 8210 MHz. (g) The sum of two WFPC2 *HST* images of 3C 368, each of duration 30 min, taken through filters F702W and F791W (see Best et al. 1997b). (h) An '*H + K*' image of 3C 368 taken using the University of Hawaii telescope with 0.3-arcsec resolution (from Stockton et al. 1996). (i-left) The magnetic field position angle, plotted wherever a rotation measure could be calculated. The contours of radio emission at 4710 MHz overlaid on figures (e) through to (i) are logarithmic with a ratio of 2, beginning at 80 μJy beam^{-1}.
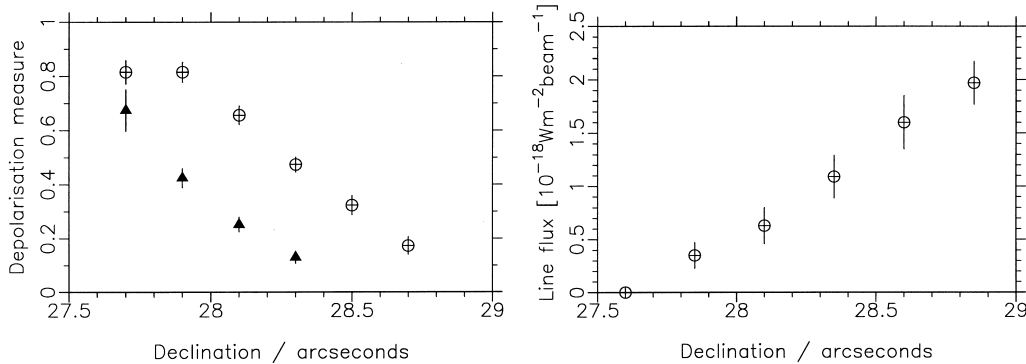
Figure 3. (a) The variation of depolarization measure with position through the southern radio lobe of 3C 368, going from south to north. The open circles show the 8210 to 4710 MHz depolarization measure, and the filled triangles show the 4710 to 1420 MHz values. (b) The variation of the [O II] emission-line flux (as measured in the observations of Meisenheimer & Hippelein 1992) over the same declination range.

The nature of the *HST* and infrared images has been extensively discussed elsewhere (Longair et al. 1995; Stockton et al. 1996; Best et al. 1997b), and we do not propose to repeat that here. We note only that the bright unresolved emission towards the centre of the *HST* image (RA 18 05 06.39, Dec. 11 01 31.3) is a foreground galactic M-dwarf star, and is thus unrelated to the structure of the radio galaxy (Hammer, Le Fèvre & Proust 1991). Assuming that the northern radio knot is the radio core, we align this with the central peak of the infrared emission from the galaxy, clearly visible in Fig. 2(h), about 1.5 arcsec north of the M star. The astrometry should be accurate to about 0.1 arcsec. The infrared and *HST* images were astrometrically aligned using the position of the M star. A number of features are now apparent from the optical and infrared images.

(i) As noted by Stockton et al. (1996), the centre of the infrared image of the galaxy coincides with a minimum in the *HST* image. We have investigated the possibility that this may be associated with a dust lane obscuring the central regions, as is frequently observed in 3CR radio galaxies at lower redshifts (de Koff et al. 1996). A model galaxy was constructed with a *K*-magnitude equivalent to that of 3C 368, $K = 17.03 \pm 0.15$, and a colour of $R - K = 5.3 \pm 0.2$, corresponding to the range expected for a passively evolving galaxy at this redshift which formed at some redshift $z_f > 3$ (Bruzual & Charlot 1993). This galaxy was constructed to have a radial intensity profile following de Vaucouleurs' law, with a characteristic radius given by the mean of those determined for the distant 3CR
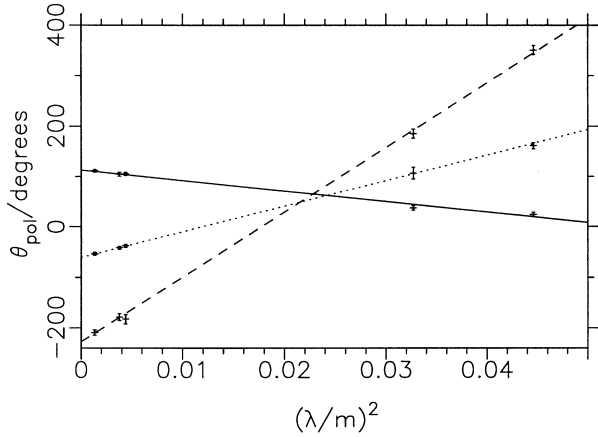
Figure 4. Fits to the polarization position angle, allowing for $n\pi$ ambiguities, versus λ^2 relation in three regions of the southern radio lobe of 3C 368: the southern region (dotted line), the north–eastern corner (dashed line) and the north–western corner (solid line).

galaxies, corresponding to $r_e = 1.7 \pm 0.4$ arcsec (Best et al. 1998).[1] The flux density expected for this model galaxy through a central 0.3-arcsec diameter aperture was then compared with that measured from the *HST* observations. We find that extinction with $E(B-V) = 0.27 \pm 0.15$ is required to obscure the central regions of the galaxy. Although only marginally significant, this value is comparable to that derived by Dickinson et al. (1996) for 3C 324. This value would be higher if some of the flux density observed from this region were associated with the aligned emission rather than with the old stellar population, as is suggested by the fairly uniform level of emission from the extended region underlying the bright optical knots.

(ii) The radio jet extending towards the northern lobe is coincident with the northern string of bright optical knots of the *HST* image. Indeed, there is a continuous optical feature running from the radio nucleus towards the hotspot. This feature undergoes a slight bend near RA 18 05 06.40, Dec. 11 01 34.2, close to a feature clearly visible in the infrared image of the galaxy. This object is significantly redder than the optical jet, and is likely to be a companion galaxy to the host of 3C 368 (Rigler et al. 1992). An interaction of the radio jet with this object may have been responsible for the brightening of the jet, as well as for the intense nebular continuum emission from this region (Dickson et al. 1995; Stockton et al. 1996).

(iii) Polarized radio emission is only detected in the region of the southern radio lobe which does not overlap with the bright optical emission; the southern hotspot shows little depolarization, even between 1.4 and 5 GHz (see Fig. 3a), whilst the region of the southern lobe close to the boundary of the optical emission shows very strong depolarization and high rotation measure gradients. No polarized emission is detected from the northern half of this lobe, even at 8 GHz. A radial decrease in the strength of the depolarization is expected if the radio source is sitting in an X-ray halo (Garrington, Conway & Leahy 1991), although for the rapid decline in depolarization seen here, the density profile of the halo would have to have a very small scale size, of order 30 kpc. Alternatively, the depolarization could involve gas associated with the radio galaxy itself; a significant proportion of the southern optical emission region of 3C 368 is associated with emission-line gas

(Meisenheimer & Hippelein 1992; Stockton et al. 1996), and large gradients in the Faraday rotation by this gas may have been responsible for depolarizing of the northern half of the southern radio lobe. In Fig. 3(b), we display the variation of the line flux of the [O II] 3727 emission line with declination, through the region of the southern lobe in which the depolarization measure changes rapidly. These data are taken from Meisenheimer & Hippelein (1992), corrected for the improved astrometry of the optical reference frames. The location of the emission line gas correlates directly with the region of strong depolarization.

If the emission line gas is responsible for this depolarization, then it must have a covering fraction, f_c, of close to unity, which allows some characteristics of the emission-line clouds to be determined. Assuming that the emission-line clouds have temperatures $T \sim 10^4$ K and are in pressure equilibrium with the hot gas in which they are embedded, they will have densities of a few times 10^7 to a few times 10^8 m^{-3}. McCarthy (1988) showed that, in the low density limit, the luminosity of the [O II] 3727 emission line could be related to the gas density and volume by the equation $L_{37} = 5.3 \times 10^{-11} n_e^2 f_v V_{64}$, where L_{37} is the luminosity of the [O II] 3727 line in units of 10^{37} W, n_e is the electron density in m^{-3}, f_v is the volume filling factor and V_{64} is the total volume in units of 10^{64} m^3. For 3C 368, $L_{37} \approx 0.8$ (Meisenheimer & Hippelein 1992, corrected for our adopted cosmology). The *HST* image indicates that the emission occurs from a region on the sky subtending about 7 by 2 arcsec^2; assuming cylindrical symmetry, $V_{64} \sim 0.04$. The above equation therefore gives a volume filling factor of between about 3×10^{-4} and 3×10^{-6}, which corresponds to a total mass of warm gas of a few times 10^8 to a few times 10^9 M$_\odot$, comparable to estimates in other radio galaxies (McCarthy 1993; Röttgering & Miley 1996). An upper limit to the sizes of the individual emission-line clouds, d, can then be calculated by $d \sim l f_v/f_c$, where $l \sim 17$ kpc is the size of the line emitting region. This upper limit is between 0.05 and 5 pc (cf. the cloud sizes of 0.035 pc derived in extended Lyα haloes by van Ojik et al. 1997).

The rotation measure is related to the gas density by the equation $RM = 8.1 \times 10^{-3} \int_0^l n_e B_\parallel dl$, where RM is measured in rad m^{-2}, n_e in m^{-3}, $B_\parallel$ in nT and l in kpc (Burn 1966). From the above calculation, the path length through the warm emission-line clouds would be a factor of between 10^4 and 10^6 lower than the path length through the surrounding hot phase gas, whilst the densities of these clouds are only a factor of 10^3 to 10^4 higher. Especially considering that the net Faraday rotation from an ensemble of cloudlets within each synthesized radio beam will get averaged down, for the warm emission-line gas to dominate the rotation measure, the magnetic fields within the cloudlets would have to be factors of at least 10 to 1000 higher than those in the surrounding hot gas phase (usually estimated at around 1 nT, e.g. Carilli et al. 1997).

Thus, if the emission-line gas is responsible for depolarizing the southern radio lobe of 3C 368 then the emission-line clouds must have a covering fraction of unity which restricts their sizes to parsec or subparsec scales, *and* the condensation of these emission-line cloudlets out of the hot gas must be accompanied by a strong amplification in the magnetic field strengths. The alternative is that the depolarization and Faraday rotation are associated with the hot cluster gas. In this case either the scale size of the X-ray halo gas would have to be co-incidently the same size as the extent of the emission-line gas, or the emission-line gas must act directly as a tracer for the region of enhanced density in the hot gaseous phase.

(iv) The southern region of emission on the *HST* image shows an elliptical structure with a central minimum. Meisenheimer & Hippelein (1992) argued that the velocity structures of the

[1]Note that due to the presence of the M star, the characteristic radius of 3C368 itself could not be determined in the work of Best et al.

emission-line gas appear consistent with this region being associated with a central bow shock caused by the radio hotspot. With our improved astrometry, for which the radio–optical correlations in the previous points have provided further support, it is apparent that the southern radio hotspot cannot coincide with this 'hole' in *HST* emission. The emission-line velocities are not associated with a bow-shock at the current position of the hotspot of the radio emission, and there is also no convincing evidence in the radio source structure for any precession of the radio source axis, whereby the radio hotspot may have advanced through this region at an earlier time. If this is truly a bow-shock structure then its origin is unclear.

(v) It is important to note that the unresolved southern radio knot is *not* coincident with the position of the M star. Many dwarf M stars display variable radio emission (White, Jackson & Kundu 1989; Spencer et al. 1993), and Hammer et al. (1991) noted that the 5-GHz flux density of this radio knot differs between the 0.45 mJy, measured by Djorgovski et al. (1987), and the 3.2 to 6.4 mJy on the radio map of Chambers et al. (1988). They argued that this radio emission might be associated with the star. This flux density 'variation' is, in reality, owing to an error in the contour labelling on the Chambers et al. map: their lobe fluxes are also a factor of 10 greater than those measured on our map. The 5-GHz flux density that we measure for the southern knot is 0.55 mJy, comparable with the value of Djorgovski et al. Furthermore, for a typical dwarf M star at a distance of 500 pc, that derived by Hammer et al. based upon the luminosity and colour of the star, the radio flux at 5 GHz even during flares would generally not exceed a few μJy, and the quiescent value would be much lower. We conclude that this southern knot is part of the radio source 3C 368 rather than arising from the M star.

4.3 The emission-line gas

The velocity structure of the emission-line gas of 3C 368 (Meisenheimer & Hippelein 1992; Stockton et al. 1996) is indicative of either infall or outflow along the radio axis, depending upon which lobe of the source is closer to us. Naively, the radio properties of the source can be used to infer the orientation of the axis relative to the line of sight. Stronger depolarization is observed in the southern lobe as compared with the northern lobe, which may be interpreted in terms of the Laing–Garrington effect (Laing 1988; Garrington et al. 1988) to imply that the southern lobe is the more distant, seen through the greater depth of material. Such a conclusion would also be consistent with the detection of a 'Doppler-boosted' one-sided radio jet in the northern arm of the source. This result would imply that the emission-line gas is infalling towards the central galaxy.

On the other hand, although the Laing–Garrington effect is almost universal in quasars, both Pedelty et al. (1989) and McCarthy, van Breugel & Kapahi (1991) find that in their samples of radio galaxies the depolarization depends more upon local environmental effects than upon orientation. We have already argued that the emission-line gas associated with the optically bright regions overlying the southern lobe may be responsible for much of the depolarization in this region. In addition, the northern lobe is strongly depolarized between 5 and 1.4 GHz (see Table 2). Furthermore, this source is not a classic jet/counter–jet example: the jet in the northern arm is weak whilst the second central knot lies in the southern arm and the southern lobe is elongated and knotty. The emission from the radio jet in the northern arm is more likely to have been brightened through its interactions with the interstellar medium than by beaming effects. We conclude, therefore, that the

radio properties are most likely dominated by environmental effects and cannot be used to indicate the orientation of 3C 368.

The tight correlation seen between the locations of bright optical and radio emission, which implies that interactions between the radio jet and its environment are of great importance in this source, argues against an infall scenario, since any infalling material would be greatly decelerated by the kinetic thrust of the radio jet. More likely is that the jet–cloud interactions would accelerate the emission line gas outwards, and produce the observed velocities as outflows (Stockton et al. 1996).

5 DISCUSSION

We summarize below the main observational results of this work.

(i) We have detected radio core candidates in each of 3C 324 and 3C 368. Aligning these relatively flat spectrum knots with the centre of the infrared images enables the radio and the optical/infrared frames of references to be astrometrically aligned to an accuracy of about 0.1 arcsec.

(ii) The radio cores of each source lie at a minimum of the optical emission, probably associated with obscuration by a central dust lane. Dust may also play an important role in determining the extended morphology of the optical emission.

(iii) Radio jets are detected in both sources, and in each case are co-linear with the strings of bright optical knots.

(iv) These observations sort out the disparity between lower angular resolution observations of the polarization structures of these radio galaxies (Pedelty et al. 1989; Fernini et al. 1993). The higher angular resolution reveals very large gradients in the rotation measure structures, reaching up to 1000 rad m^{-2} over a distance of order 10 kpc, and regions of strong depolarization.

(v) There is a tight correlation between the depolarization measures and the gradients in the rotation measure, suggesting that the depolarization is external, and caused by variations within each beamwidth of the Faraday depth of material in the vicinity of the radio source.

The striking co-linearity of the radio jet with the bright optical knots in the two sources indicate that interactions of the radio jet itself, rather than just the AGN or the radio cocoon, must play a critical role in the origin of the aligned optical emission. Of interest is that, given these strong interactions between the radio jets and their environment, more enhanced radio emission is not seen in these regions, in contrast to that observed in bright radio knots at the sites of jet–cloud interactions at low redshifts (e.g. 4C 29.30, van Breugel et al. 1986). This suggests that the more powerful radio jets in these high redshift sources are not as strongly disrupted by their interactions.

Despite the many similarities between the two sources, there are equally important differences. The northern arm of 3C 368 shows a tight correlation between the regions of radio and optical emission, whilst in 3C 324 although these are co-linear they are not co-spatial. The nature of the optical (rest-frame ultraviolet) emission of the two galaxies is also very different. 3C 324 has a high percentage of spatially extended optical polarization, $P \approx 11$ per cent, indicating that illumination by the central AGN must be important in this source (Cimatti et al. 1996). In contrast, *HST* and Keck observations of 3C 368 have detected no polarized optical emission (van Breugel 1996).

3C 368 is an exceptional source, being probably the most aligned of all of the 3CR radio galaxies and possessing the highest emission line flux. The extent of its radio emission is 73 kpc, only slightly

greater than that of the optical emission. Its structure may be interpreted in terms of it being a relatively young radio source (a few times 10^6 yr), in which on-going interactions between the radio jet and the interstellar medium remain the dominant effects. In the northern region of this source, where the bright optical knots lie coincident with the radio jet, the nebular continuum emission is very luminous and the emission-line velocities are high (Dickson et al. 1995; Stockton et al. 1996). Interactions between the radio jet and its environment, possibly including a companion galaxy (see Section 4.2) may brighten the radio jet and accelerate and shock-ionize the warm emission-line gas, explaining all of these features. The strong correlation between the radio and optical structures cannot be explained if the gas responsible for the nebular continuum is photoionized by the AGN. Jet-induced star formation in this region cannot be excluded, but there is no direct evidence for this. Any small contribution of scattered light might not be detectable owing to the dilution of the polarization by the very strong nebular continuum contribution.

The radio emission of 3C 324 is more extended and reaches well beyond the region of bright optical emission. In this source, we may be observing the residual effects after the radio jets have forced a passage through the host galaxy. In the aftermath of the jet shocks the nebular continuum contribution has decreased, and now some scattered light is detected. Cimatti et al. (1996) calculate that at most 30 to 50 per cent of the optical flux density can be associated with scattered radiation, with the rest likely to be nebular continuum emission or light from a young starburst. They suggest that the knot close to the western lobe may currently be undergoing a burst of star formation at a rate of $70\,M_\odot\,yr^{-1}$. Most of the optical emission from 3C 324 arises from the bright knotty structures along the radio axis, with no evidence for the scattered emission being evenly distributed over an ionization cone structure. Therefore, the scattering material in this source must also be preferentially located along the jet direction. Two possible mechanisms for this latter effect would the production of dust in a region of star formation induced by the radio jet, or the disintegration of cooled clumps of optically thick gas by the jet, and the exposure of previously hidden dust grains at their centre (Bremer et al. 1997).

At low redshifts, rotation measure values and variations in excess of a few hundred rad m^{-2} are seen in two types of radio source, compact steep spectrum radio sources in which the radio lobes lie within the host galaxy (e.g. Taylor, Inoue & Tabara 1992), and FR II radio sources located in clusters with luminous X–ray cooling flows. For the former, Garrington & Akujor (1996) have suggested that the rotation measure correlates with linear size, with the dense gas located towards the centre of the host galaxy being responsible for the Faraday rotation. For the latter, Taylor et al. (1994) found a correlation between the rotation measure and the cooling flow rate, suggesting that the intracluster medium is responsible.

We have argued that the large rotation measures observed in the southern lobe of 3C 368 are due to emission-line gas associated with the host galaxy. The northern lobe of this source, however, and both lobes of 3C 324, lie distant from the host galaxy. Dickinson (1997) has reported the detection of extended X-ray emission at a luminosity of $L_X = (8.1 \pm 1.6) \times 10^{44}\,erg\,s^{-1}$ from 3C 324, a value comparable to that of the Coma cluster. He associates this with cooling intracluster gas. Similarly, 3C 368 has been detected using the *ROSAT* PSPC, with a signal-to-noise ratio of 5, giving $L_X \sim 1.7 \times 10^{44}\,erg\,s^{-1}$ (Crawford & Fabian 1995). If these X-ray luminosities are associated with cooling flows, then the cooling flow rates and rotation measures lie roughly upon the correlation of Taylor et al. (1994), suggesting that the high rotation measures of

3C 324 and of the regions of 3C 368 away from the emission line gas are indeed associated with their intracluster gas. These rotation measure values are not as extreme as, for example, the $20\,000$ rad m^{-2} seen in 3C 295, at the centre of a very rich cluster of galaxies at $z = 0.461$ (Perley & Taylor 1991), but the large values and gradients provide further support for the hypothesis that powerful distant radio galaxies lie in at least moderately rich young cluster environments.

REFERENCES

Athreya R. M., Kapahi V. K., McCarthy P. J., van Breugel W. J. M., 1997, MNRAS, 289, 525
Best P. N., Longair M. S., Röttgering H. J. A., 1996, MNRAS, 280, L9
Best P. N., Longair M. S., Röttgering H. J. A., 1997a, MNRAS, 286, 785
Best P. N., Longair M. S., Röttgering H. J. A., 1997b, MNRAS, 292, 758
Best P. N., Longair M. S., Röttgering H. J. A., 1998, MNRAS, 295, 549
Bremer M. N., Fabian A. C., Crawford C. S., 1997, MNRAS, 284, 213
Brodie J., Bowyer S., McCarthy P. J., 1985, ApJ, 293, L59
Bruzual G., Charlot S., 1993, ApJ, 405, 538
Burn B. J., 1966, MNRAS, 133, 67
Carilli C. L., Owen F. N., Harris D. E., 1994, AJ, 107, 480
Carilli C. L., Röttgering H. J. A., van Ojik R., Miley G. K., van Breugel W. J. M., 1997, ApJS, 109, 1
Chambers K. C., Miley G. K., Joyce R. R., 1988, ApJ, 329, L75
Chambers K. C., Miley G. K., van Breugel W. J. M., 1987, Nat, 329, 604
Cimatti A., Dey A., van Breugel W., Antonucci R., Spinrad H., 1996, ApJ, 465, 145
Cimatti A., Dey A., van Breugel W., Hurt T., Antonucci R., 1997, ApJ, 476, 677
Cox C. I., Gull S. F., Scheuer P. A. G., 1991, MNRAS, 252, 558
Crawford C. S., Fabian A. C., 1995, MNRAS, 273, 827
Crawford C. S., Fabian A. C., 1996, MNRAS, 282, 1483
de Koff S., Baum S. A., Sparks W. B., Biretta J., Golombek D., Macchetto F., McCarthy P., Miley G. K., 1996, ApJS, 107, 621
Dey A., Spinrad H., 1996, ApJ, 459, 133
Dey A., van Breugel W. J. M., Vacca W. D., Antonucci R., 1997, ApJ, 490, 698
Dickinson M., 1997, in Tanvir N. R., Aragón-Salamanca A., Wall J. V., eds, *HST* and the high redshift Universe. World Scientific, Singapore, p. 207
Dickinson M., Dey A., Spinrad H., 1996, in Hippelein H., Meisenheimer K., Röser H.-J., eds, Galaxies in the Young Universe. Springer Verlag, Berlin, p. 164
Dickson R., Tadhunter C., Shaw M., Clark N., Morganti R., 1995, MNRAS, 273, L29
Djorgovski S., Spinrad H., Pedelty J., Rudnick L., Stockton A., 1987, AJ, 93, 1307
Dreher J. W., Carilli C. L., Perley R. A., 1987, ApJ, 316, 611

Dunlop J. S., Peacock J., 1993, MNRAS, 263, 936

Eisenhardt P., Chokshi A., 1990, ApJ, 351, L9

Fernini I., Burns J. O., Bridle A. H., Perley R. A., 1993, AJ, 105, 1690

Garrington S. T., Akujor C. E., 1996, in Ekers R., Fanti C., Padrielli L., eds, Proc. IAU Symp. 175, Extragalactic radio sources. Kluwer Academic Publishers, Dordrecht, p. 77

Garrington S. T., Conway R. G., Leahy J. P., 1991, MNRAS, 250, 171

Garrington S. T., Leahy J. P., Conway R. G., Laing R. A., 1988, Nat, 331, 147

Hammer F., Le Fèvre O., Proust D., 1991, ApJ, 374, 91

Johnson R. A., Leahy J. P., Garrington S. T., 1995, MNRAS, 273, 877

Laing R. A., 1988, Nat, 331, 149

Laing R. A., Riley J. M., Longair M. S., 1983, MNRAS, 204, 151

Lattanzi M. G., Capetti A., Macchetto F. D., 1997, A&A, 318, 997

Leahy J. P., 1987, MNRAS, 226, 433

Liu R., Pooley G., 1991, MNRAS, 249, 343

Longair M. S., Best P. N., Röttgering H. J. A., 1995, MNRAS, 275, L47

Lonsdale C. J., Barthel P. D., Miley G. K., 1993, ApJS, 87, 63

McCarthy P. J., 1988, PhD thesis, Univ. of California, Berkeley

McCarthy P. J., 1993, ARA&A, 31, 639

McCarthy P. J., van Breugel W. J. M., Kapahi V. K., 1991, ApJ, 371, 478

McCarthy P. J., van Breugel W. J. M., Spinrad H., Djorgovski S., 1987, ApJ, 321, L29

Meisenheimer K., Hippelein H., 1992, A&A, 264, 455

Pedelty J. A., Rudnick L., McCarthy P. J., Spinrad H., 1989, AJ, 97, 647

Pentericci L., Röttgering H. J. A., Miley G. K., Carilli C. L., McCarthy P. J., 1997, A&A, 326, 580

Perley R. A., Taylor G. B., 1991, AJ, 101, 1623

Rees M. J., 1989, MNRAS, 239, 1P

Rigler M. A., Lilly S. J., Stockton A., Hammer F., Le Fèvre O., 1992, ApJ, 385, 61

Röttgering H. J. A., Miley G. K., 1996, in Bergeron J., ed., The Early Universe with the VLT. Springer Verlag, Berlin, p. 285

Scheuer P. A. G., Williams P. J. S., 1968, ARA&A, 6, 321

Shepherd M. C., 1997, in Hunt G., Payne H. E., eds, ASP Conf. Ser. 125, Astronomical Data Analysis Software and Systems VI. Astron. Soc. Pac., San Francisco p. 77

Spencer R. E., Davis R. J., Zafiropoulos B., Nelson R. F., 1993, MNRAS, 265, 231

Stockton A., Ridgway S. E., Kellogg M., 1996, AJ, 112, 902

Tadhunter C. N., Dickson R., Morganti R., Villar-Martin M., 1997, in Clements D. L., Pérez-Fournon I., eds, Quasar Hosts. Springer-Verlag, Berlin, p. 311

Taylor G. B., Inoue M., Tabara H., 1992, A&A, 264, 421

Taylor G. B., Barton E. J., Ge J. P., 1994, AJ, 107, 1942

Tribble P. C., 1991, MNRAS, 250, 726

van Breugel W. J. M., 1996, in Ekers R., Fanti C., Padrielli L., eds, Proc. IAU Symp. 175, Extragalactic radio sources. Kluwer Academic Publishers, Dordrecht, p. 577

van Breugel W. J. M., Dey A., 1993, ApJ, 414, 563

van Breugel W. J. M., Filippenko A. V., Heckman T. M., Miley G. K., 1985, ApJ, 293, 83

van Breugel W. J. M., Heckman T. M., Miley G. K., Filippenko A. V., 1986, ApJ, 311, 58

van Ojik R., Röttgering H. J. A., Miley G. K., Hunstead R., 1997, A&A, 317, 358

White S. M., Jackson P. D., Kundu M. R., 1989, ApJS, 71, 895

Yates M. G., Miller L., Peacock J. A., 1989, MNRAS, 240, 129

This paper has been typeset from a T$_E$X/L^{A}T$_E$X file prepared by the author.